Polyoxometalates

DOI: 10.1002/anie.201007617

A Planar $\{Mn_{19}(OH)_{12}\}^{26+}$ Unit Incorporated in a 60-Tungsto-6-Silicate Polyanion**

Bassem S. Bassil, Masooma Ibrahim, Rami Al-Oweini, Marie Asano, Zhenxing Wang, Johan van Tol, Naresh S. Dalal, Kwang-Yong Choi, Rosa Ngo Biboum, Bineta Keita, Louis Nadjo, and Ulrich Kortz**

Polyoxometalates (POMs) are discrete metal–oxo anions of early transition-metals in high oxidation states (e.g. W^{VI}, Mo^{VI}, V^{V}) and they are usually synthesized in aqueous, acidic medium.[1] Most classical POMs are based on edge- and corner-shared MO_6 octahedra. However, the recently discovered POM subclass of noble metalates comprises linked square-planar MO_4 units ($M = Pd^{II}$, Au^{III}).[2] Lacunary (vacant) POMs can be considered as inorganic, multidentate ligands, and hence they are good candidates for the encapsulation of large, multinuclear d- and f-block metal–oxo fragments, sometimes resulting in compounds with interesting magnetic properties.[3]

A pioneering result in this area was the synthesis of $[Mn_{12}(CH_3COO)_{16}(H_2O)_4O_{12}]$ (**Mn_{12}**) by Lis in 1980, which was shown to exhibit single-molecule magnet (SMM) behavior by Gatteschi's group 13 years later.[4] During the past two decades many high-nuclearity, transition-metal based, coordination complexes with interesting electronic and magnetic properties have been prepared.[5] High-nuclearity manganese complexes have been amongst the most studied in this class, and there are examples containing up to 84 manganese ions.[4,6]

To date there are only a few high-nuclearity manganese–oxo-containing POMs, such as $\{[XW_9O_{34}]_2[Mn^{III}_4Mn^{II}_2O_4(H_2O)_4]\}^{12-}$ ($X = Si$, Ge)[7a] and $[Mn^{III}_{13}Mn^{II}O_{12}(PO_4)_4(PW_9O_{34})_4]^{31-}$.[7b]

Herein we report the synthesis and structure as well as the magnetic and electrochemical properties of a 19 manganese(II) center containing 60-tungsto-6-silicate, $[Mn_{19}(OH)_{12}(SiW_{10}O_{37})_6]^{34-}$ (**1**), which was isolated as a hydrated sodium salt, $Na_{34}[Mn_{19}(OH)_{12}(SiW_{10}O_{37})_6]\cdot 115\,H_2O$ (Na-**1**).

Single-crystal X-ray diffraction[8] revealed that polyanion **1** consists of a cationic $\{Mn_{19}(OH)_{12}\}^{26+}$ (Mn_{19}) assembly stabilized by six dilacunary $[\alpha\text{-}SiW_{10}O_{37}]^{10-}$ units resulting in a structure with S_6 point-group symmetry (Figure 1, top). To the best of our knowledge, **1** is the highest nuclearity manganese-containing POM known to date. All 19 Mn^{II} ions lie in the same plane forming a hexagonal structure based on edge-shared MnO_6 octahedra. The Mn^{II} ions in Mn_{19} are connected by a total of twelve μ_3-hydroxo bridges, as determined by bond valence sum (BVS) calculations (Supporting Information, Table S1).[9] The discrete Mn_{19} nanosheet (Figure 1, bottom) is held in place by six dilacunary $[\alpha\text{-}SiW_{10}O_{37}]^{10-}$ units through μ_4-, μ_3-, and μ_2-oxo bridges. The central Mn^{II} ion in Mn_{19} is hexacoordinated in a regular octahedral fashion with average Mn–O bond lengths of 2.21(4) Å. This unique Mn^{II} ion is bridged to the six surrounding Mn^{II} ions by six hydroxo bridges, resulting in a compact Mn_7 core-fragment resembling the Anderson–Evans structure type.[10] This fragment has a hexagonally closest-packed brucite structure, in which the Mn^{II} ions are located in the octahedral holes. This type of Mn_7 core aggregate has been observed in several coordination complexes.[5,6a,11]

Interestingly, all of these six outer Mn^{II} ions are heptacoordinated, each with four "normal" Mn–O bonds (ca. 2.1–2.2 Å) and three long Mn–O bonds (ca. 2.4–2.6 Å). BVS calculations reveal a combined contribution of approximately 1.5 bond valences from the four shorter bonds and 0.5 from the three longer ones, resulting in the expected total bond valence of 2.0 for each of the six Mn^{II} ions (Supporting Information, Table S1). Heptacoordination for Mn^{II} is not unusual in coordination chemistry.[12] The Mn_7 core is surrounded by a ring of 12 Mn^{II} ions, which are all hexacoordinated in a distorted octahedral fashion with Mn–O bond lengths ranging from 2.02(3) to 2.37(2) Å. These 12 outer Mn^{II}

[*] Dr. B. S. Bassil,[+] M. Ibrahim,[+] R. Al-Oweini, M. Asano, Prof. U. Kortz
Jacobs University, School of Engineering and Science
P.O. Box 750561, 28725 Bremen (Germany)
Fax: (+49) 421-200-3229
E-mail: u.kortz@jacobs-university.de
Homepage: http://www.jacobs-university.de/ses/ukortz

Z. Wang, Dr. J. van Tol, Prof. N. S. Dalal
Department of Chemistry and Biochemistry
National High Magnetic Field Laboratory
Florida State University, Tallahassee, FL 32306 (USA)
E-mail: dalal@chem.fsu.edu

Prof. K.-Y. Choi
Department of Physics, Chung-Ang University
Seoul 156-756 (Republic of Korea)

R. Ngo Biboum, Dr. B. Keita, Prof. L. Nadjo
Laboratoire de Chimie Physique
Université Paris-Sud 11, 91405 Orsay Cedex (France)

[+] These authors contributed equally to this work.

[**] U.K. thanks the German Science Foundation (DFG-KO-2288/3-2), Jacobs University and the Fonds der Chemischen Industrie for research support. M.I. thanks DAAD and the Higher Education Commission of Pakistan for a doctoral fellowship, and the University of Balochistan, Quetta, Pakistan for allowing her to pursue PhD studies at Jacobs University (Germany). NHMFL is supported by the State of Florida and the NSF Cooperative agreement No. DMR 0654118. K.-Y. C. acknowledges financial support from Korea NRF (Grant No. 2009-0093817). Figure 1 was generated by Diamond Version 3.2c (copyright Crystal Impact GbR).

Supporting information for this article is available on the WWW under http://dx.doi.org/10.1002/anie.201007617.

© 2011 Wiley-VCH Verlag GmbH & Co. KGaA, Weinheim

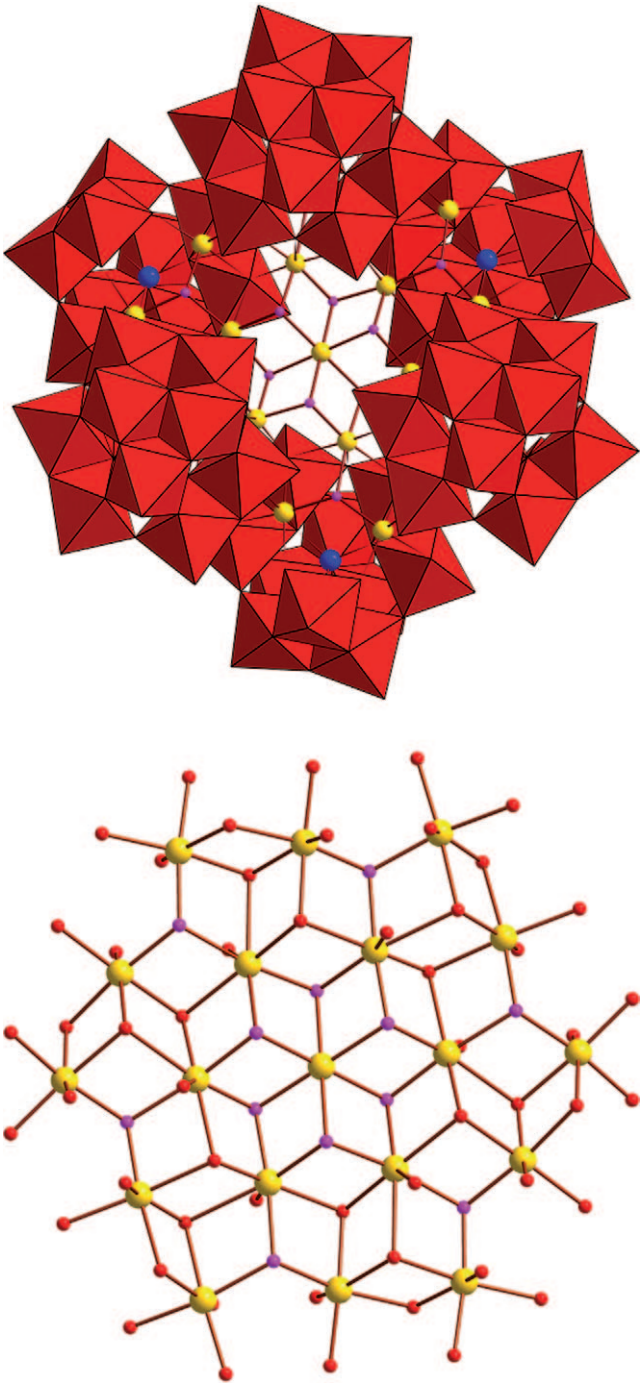

Figure 1. Top: Combined polyhedral/ball-and-stick representation of **1**. Bottom: Ball-and-stick representation of the Mn_{19}-oxo-hydroxo core in **1**. Protonated oxygen atoms are shown in pink. WO_6 red octahedra, Si blue balls, Mn yellow balls, O red balls.

ions are arranged in six edge-shared pairs, each filling the lacunary sites of the six $[\alpha\text{-}SiW_{10}O_{37}]^{10-}$ units. Thermogravimetric analysis (TGA) of Na-**1** gave 115 waters of crystallization (Supporting Information, Figure S1), which is consistent with elemental analysis (see below).

Notably, in 2001 Westin's group also reported a planar Mn_{19} magnetic core in an oxo–alkoxide complex, $[Mn_{19}O_{12}(moe)_{14}(moeH)_{10}]$ ({Mn_{19}org}, see Supporting Information, Figure S2), which was synthesized in an inert atmosphere by reaction of $MnCl_2$ with potassium methoxyethoxide in toluene/$HOC_2H_4OCH_3$.[13] This Mn_{19} assembly is in fact very similar, but not identical, to that of **1**. The magnetic properties of {Mn_{19}org} were investigated by Gatteschi's group and modeled using the Monte Carlo method.[14] Moreover, Powell's group synthesized an Fe_{19}-containing coordination complex stabilized by chelating NOOO ligands.[5b]

A number of synthetic factors play a significant role in the formation of polyanion **1**, such as the type of reactant salt, ratio of reactants, pH value, temperature, and solvent. The synthesis of polyanion **1** is only successful when starting with the sodium salt of the trilacunary precursor $[A\text{-}\alpha\text{-}SiW_9O_{34}]^{10-}$ and if no other countercations are present in solution during the reaction. An extra tungsten center is inserted into $[A\text{-}\alpha\text{-}SiW_9O_{34}]^{10-}$ in situ, as a result of partial decomposition of some of the lacunary POM precursor in solution. Interestingly, addition of one equivalent of sodium tungstate at any point during the reaction did not result in **1**.

The synthesis of **1** consists of two steps. The first step involves reaction of Mn^{II} ions with the trilacunary precursor $[A\text{-}\alpha\text{-}SiW_9O_{34}]^{10-}$ at room temperature and pH 8 for about 30 min, and the second step involves addition of sodium phosphate while keeping the pH at 8, followed by moderate heating of the solution for around 1 h. These two steps appear to be crucial for the successful synthesis of polyanion **1**. If the reaction is performed directly in phosphate buffer, **1** is not formed. The pH value is also critical, as pH < 7 or pH > 9 does not lead to the formation of **1**. The temperature of step 2 is also crucial, as the yield improves with increasing temperature, but above 70 °C an unidentified, black-brown side-product is formed. Also, step 2 seems to work only in sodium phosphate buffer. Efforts to reproduce polyanion **1** by addition of CH_3COONa, Na_2CO_3, or NaCl instead of Na_3PO_4 to the reaction mixture, while keeping the pH value at 8, were all unsuccessful. All this reflects the difficulty of rationalizing the mechanistic pathways of POM formation.

We have also investigated the electrochemistry of **1** in aqueous solution (see Supporting Information for details). In short, the reduction of **1** in pH 5 medium gives two well-defined waves assigned to tungsten located at −0.850 V and −0.960 V versus the saturated calomel electrode (SCE; Supporting Information, Figure S3). Controlled potential coulometry indicates that the reduced form associated with the first tungsten redox couple is already active for the hydrogen evolution reaction. The first step of Mn^{II} oxidation proceeds to the Mn^{IV} state via the Mn^{III} state, in agreement with previous results.[15a] Controlled potential coulometry indicates that all the manganese centers are electroactive and have a +2 oxidation state.

Finally, a new, very intense oxidation wave is observed at more positive potential values (Supporting information, Figure S4). This wave is mainly attributed to the oxygen evolution reaction (OER) from water.[15a] Taking into account the diversity of reported experimental conditions, **1** displays very competitive kinetic parameters for the OER: 1) a good linearity was observed between an overpotential of 330 mV to 600 mV (Supporting Information, Figure S4), this observation coincides roughly with two remarkable results obtained

 © 2011 Wiley-VCH Verlag GmbH & Co. KGaA, Weinheim

recently for nanotubes decorated with a ruthenium-containing POM[15b] and for a catalyst containing phosphate and Co^{II}.[15c] 2) in contrast, the slope of the Tafel line ((135 ± 10) mV) lies in-between those which could be estimated from these reports (310 mV [15b] and 83 mV [15c]). Thus, **1** shows better OER kinetics than the ruthenium-containing POM. 3) The exchange current density, i_0, expressed in $A\,cm^{-2}$ ($\log i_0 = -6.8 \pm 0.2$) compares favorably with analogous reported values.[15c] The efficiency of **1** might be attributed to its multiple μ-hydroxo/oxo bridging units connecting adjacent metal centers, a situation analogous to that in the $CaMn_4O_4$ cluster used by nature to oxidize water at low overpotential.

The Mn_{19} core in polyanion **1** is of interest for its magnetic properties, as this structure presents an intermediate between an infinite, two-dimensional, spin-frustrated, triangular lattice and a small molecular complex with a well-defined spin ground state. Spin-frustrated triangular lattices show a variety of phase transitions and magnetic structures.[16,17] As mentioned above, the magnetic properties of Westin's organic-capped coordination complex {Mn_{19}org} have been investigated, but the EPR measurements were reported to be somewhat problematic because of saturation effects.[14] Extensive Monte Carlo simulations of the magnetic susceptibility showed that the magnetic properties of {Mn_{19}org} are dominated by strong antiferromagnetic interactions ($J = -24$ K) between the seven central Mn^{II} ions, with a ground state of $S = 5/2$. The role of the other, peripheral 12 Mn^{II} ions was minor.

Our motivation was to study the magnetic and EPR properties of the Mn_{19} assembly in polyanion **1**, comparing them with those of {Mn_{19}org} and examining if the inorganic ligands in **1** modify the magnetic properties of the Mn_{19} core. We carried out detailed EPR measurements over the frequency range 54–432 GHz and the temperature range 3–285 K, magnetic susceptibility over 1.8–300 K and magnetization measurements in an applied field of 0–7 T. The SQUID data yielded a $\chi_m T$ value of 85.04 emu K mol^{-1} at room temperature, close to the expected value (83.125 emu K mol^{-1} taking $g_{av} = 2$) for 19 uncoupled Mn^{II} ions ($S = 5/2$). Upon lowering the temperature, the value of $\chi_m T$ decreased gradually owing to the development of antiferromagnetic correlations. At the lowest temperatures, the spin state corresponds approximately to a total spin of $S = 5/2$ for the Mn_{19} unit (Supporting Information, Figure S5). However, the finer details of the magnetization and susceptibility curves could not be fully simulated, because of the complexity of this large complex with its competing exchange interactions.

Figure S6 in the Supporting Information shows the spin topology of the Mn_{19} core in **1**. The 19 exchange-coupled Mn^{II} ions ($S = 5/2$) form a distorted, finite, two-dimensional triangular spin lattice with 21 slightly different exchange interactions. Since a Hilbert space of $6^{19} = 6.09 \times 10^{14}$ is huge, the magnetic behavior of the Mn_{19} core would be described by a classical Heisenberg model in a continuum limit $\hat{H} = J_{ij} S_i S$. This conjecture was fully supported by our EPR measurements over a broad temperature and microwave-frequency range as stated above. Under all conditions, only a single, inhomogeneously broadened peak was observed, without any sign of fine structure or hyperfine splitting (Supporting information, Figure S7).

As the magnetic field increases, a gradual increase of the ground spin state and $\langle S_z \rangle$ is observed well below 7 T. Even at 1.8 K, no steps are observed in the magnetization. It is therefore an open question whether this system can be described by a series of discrete spin states, or if a description in terms of a continuum is more appropriate, somewhat reminiscent of short-range order in an infinite two-dimensional lattice. We note that our magnetic susceptibility data do not exhibit a round maximum, in contrast to {Mn_{19}org}, where a maximum was found at 12 K. The absence of a round maximum for **1** shows that its 21 antiferromagnetic J values are more or less continuously spread, leaving just one free Mn^{II} ($S = 5/2$) ion to control the magnetism of the ground state. This is the reason for the nonlinearity of the magnetization curve in Figure S8B (Supporting Information) for **1**, while no such nonlinearity was reported for {Mn_{19}org}. Regarding a magnetic comparison of **1** with {Mn_{21}},[6a] {Mn_{21}} consists of a {$Mn^{IV}{}_9O_{20}$} sheet held within a nonplanar {$Mn^{III}{}_{12}O_{12}$} ring, whereas the {$Mn_{19}(OH)_{12}$} core of **1** consists exclusively of Mn^{II} ions, and is essentially planar. Thus, it is very difficult to compare these two compounds.

In summary, we have prepared the novel, discrete polyanion **1**, comprising a cationic, planar $\{Mn_{19}(OH)_{12}\}^{26+}$ assembly incorporated in a 60-tungsto-6-silicate, by reaction of Mn^{II} ions with $[A\text{-}\alpha\text{-}SiW_9O_{34}]^{10-}$ in aqueous solution at room temperature. This approach is made possible by performing the reaction at pH 8, which is unusual in polyanion synthesis. The planar Mn_{19} magnetic cluster in **1** is unprecedented in POM chemistry, and in fact **1** contains more manganese ions than any other polyanion reported to date. A comparison of the structural and magnetic aspects of the inorganic capped Mn_{19} assembly in **1** with the organic capped {Mn_{19}org} exhibited significant differences. This result indicates a large potential for the preparation of polyanion capped analogues of the many known multinuclear, magnetic coordination complexes.[4,6] Here we have demonstrated that it is also possible to prepare unexpectedly large, magnetic metal–oxo assemblies using simple metal salts, without the need for multinuclear coordination complex precursors or cyclic, robust polyanion templates, such as $\{P_8W_{48}\}$.[18] Using the synthetic methodology described herein we have already prepared {Mn_8}, {Ni_{14}}, {Cu_{15}}, and {Co_{16}}[19] polyanions, which will be reported elsewhere.

Experimental Section

$Na_{34}[Mn_{19}(OH)_{12}(SiW_{10}O_{37})_6]\cdot 115\,H_2O$ (Na-**1**): $MnCl_2\cdot 4\,H_2O$ (0.13 g, 0.63 mmol) was dissolved in H_2O (20 mL). Then solid $Na_{10}[A\text{-}\alpha\text{-}SiW_9O_{34}]$[20] (0.50 g, 0.20 mmol) was added and stirred until a clear yellow solution was obtained. The pH value of the resulting mixture was adjusted to 8 with 4 M NaOH. The turbid solution was stirred for 30 min at room temperature. Then solid Na_3PO_4 (0.50 g, 3.0 mmol) was added to this solution in small portions, while maintaining the pH at 8 with HCl_{aq}. The mixture was heated to 70 °C for 1 h, allowed to cool to room temperature, and then filtered. The filtrate was allowed to evaporate in an open vial at room temperature. After two weeks a brown crystalline product started to appear. Evaporation was allowed to continue until the solution level had approached the solid product,

 © 2011 Wiley-VCH Verlag GmbH & Co. KGaA, Weinheim

which was then collected by filtration and air dried. Yield 0.040 g (6.5%).

IR (2% KBr pellet): $\tilde{\nu}$ = 988 (w), 945 (m), 890 (s), 790 (s), 707 (m), 650 (m), 535 cm^{-1} (m), see Figure S9. Elemental analysis for Na-**1**, calcd: Na 4.1, Si 0.89, Mn 5.54, W 58.5; found: Na 4.2, Si 0.86, Mn 5.61, W 59.1.

Received: December 5, 2010
Revised: March 25, 2011
Published online: May 17, 2011

Keywords: electrochemistry · magnetic properties · manganese · polyoxometalates · structure elucidation

[1] a) A. Müller, S. Roy, *Coord. Chem. Rev.* **2003**, *245*, 153–166; b) E. Coronado, P. Day, *Chem. Rev.* **2004**, *104*, 5419–5448; c) L. Cronin in *Comprehensive Coordination Chemistry* II, *Vol. 7* (Eds.: J. A McCleverty, T. J. Meyer), Elsevier, Amsterdam, **2004**, pp. 1–57; d) B. Hasenknopf, K. Micoine, E. Lacôte, S. Thorimbert, M. Malacria, R. Thouvenot, *Eur. J. Inorg. Chem.* **2008**, 5001–5013; e) Issue dedicated to Polyoxometalates; Guest Ed. U. Kortz, *Eur. J. Inorg. Chem.* **2009**, *34*; f) D.-L. Long, R. Tsunashima, L. Cronin, *Angew. Chem.* **2010**, *122*, 1780–1803; *Angew. Chem. Int. Ed.* **2010**, *49*, 1736–1758.

[2] a) E. V. Chubarova, M. H. Dickman, B. Keita, L. Nadjo, F. Miserque, M. Mifsud, I. W. C. E. Arends, U. Kortz, *Angew. Chem.* **2008**, *120*, 9685–9689; *Angew. Chem. Int. Ed.* **2008**, *47*, 9542–9546; b) N. V. Izarova, N. Vankova, T. Heine, R. Ngo Biboum, B. Keita, L. Nadjo, U. Kortz, *Angew. Chem.* **2010**, *122*, 1930–1933; *Angew. Chem. Int. Ed.* **2010**, *49*, 1886–1889; c) N. V. Izarova, N. Vankova, A. Banerjee, G. B. Jameson, T. Heine, F. Schinle, O. Hampe, U. Kortz, *Angew. Chem.* **2010**, *122*, 7975–7980; *Angew. Chem. Int. Ed.* **2010**, *49*, 7807–7811; d) M. Barsukova, N. V. Izarova, R. Ngo Biboum, B. Keita, L. Nadjo, V. Ramachandran, N. S. Dalal, N. S. Antonova, J. J. Carbó, J. M. Poblet, U. Kortz, *Chem. Eur. J.* **2010**, *16*, 9076–9085; e) M. Barsukova-Stuckart, N. V. Izarova, G. B. Jameson, V. Ramachandran, Z. Wang, J. van Tol, N. S. Dalal, R. Ngo Biboum, B. Keita, L. Nadjo, U. Kortz, *Angew. Chem.* **2011**, *123*, 2688–2692; *Angew. Chem. Int. Ed.* **2011**, *50*, 2639–2642.

[3] a) E. Coronado, C. Giménez-Saiz, C. J. Gómez-García, V. Laukhin, *Nature* **2000**, *408*, 447–449; b) E. Coronado, C. Giménez-Saiz, C. J. Gómez-García, *Coord. Chem. Rev.* **2005**, *249*, 1776–1796; c) X. Fang, P. Kögerler, *Chem. Commun.* **2008**, 3396–3398; d) U. Kortz, A. Müller, J. van Slageren, J. Schnack, N. S. Dalal, M. Dressel, *Coord. Chem. Rev.* **2009**, *253*, 2315–2327.

[4] a) T. Lis, *Acta Crystallogr. Sect. B* **1980**, *36*, 2042–2046; b) R. Sessoli, D. Gatteschi, A. Caneschi, M. A. Novak, *Nature* **1993**, *365*, 141–143.

[5] Representative examples: a) S. L. Heath, A. K. Powell, *Angew. Chem.* **1992**, *104*, 191–192; *Angew. Chem. Int. Ed. Engl.* **1992**, *31*, 191–193; b) A. K. Powell, S. L. Heath, D. Gatteschi, L. Pardi, R. Sessoli, G. Spina, F. Del Giallo, F. Pierallill, *J. Am. Chem. Soc.* **1995**, *117*, 2491–2502; c) E. K. Brechin, S. G. Harris, A. Harrison, S. Parsons, A. G. Whittaker, R. E. P. Winpenny, *Chem. Commun.* **1997**, 653–654; d) M. Murugesu, R. Clérac, W. Wernsdorfer, C. E. Anson, A. K. Powell, *Angew. Chem.* **2005**, *117*, 6836–6840; *Angew. Chem. Int. Ed.* **2005**, *44*, 6678–6682.

[6] Representative examples: a) J. T. Brockman, J. C. Huffman, G. Christou, *Angew. Chem.* **2002**, *114*, 2616–2618; *Angew. Chem. Int. Ed.* **2002**, *41*, 2506–2508; b) C. Cañada-Vilalta, M. Pink, G. Christou, *Dalton Trans.* **2003**, 1121–1125; c) Y. Li, W. Wernsdorfer, R. Clérac, I. J. Hewitt, C. E. Anson, A. K. Powell, *Inorg. Chem.* **2006**, *45*, 2376–2378; d) A. M. Ako, I. J. Hewitt, V. Mereacre, R. Clérac, W. Wernsdorfer, C. E. Anson, A. K. Powell, *Angew. Chem.* **2006**, *118*, 5048–5051; *Angew. Chem. Int. Ed.* **2006**, *45*, 4926–4929; e) J. T. Brockman, T. C. Stamatatos, W. Wernsdorfer, K. A. Abboud, G. Christou, *Inorg. Chem.* **2007**, *46*, 9160–9171; f) T. C. Stamatatos, K. A. Abboud, W. Wernsdorfer, G. Christou, *Angew. Chem.* **2007**, *119*, 902–906; *Angew. Chem. Int. Ed.* **2007**, *46*, 884–888; g) E. Ruiz, T. Cauchy, J. Cano, R. Costa, J. Tercero, S. Alvarez, *J. Am. Chem. Soc.* **2008**, *130*, 7420–7426.

[7] a) C. Ritchie, A. Ferguson, H. Nojiri, H. N. Miras, Y. Song, D. Long, E. Burkholder, M. Murrie, P. Kögerler, E. K. Brechin, L. Cronin, *Angew. Chem.* **2008**, *120*, 5691–5694; *Angew. Chem. Int. Ed.* **2008**, *47*, 5609–5612; b) Q. Wu, Y. Li, Y. Wang, E. Wang, Z. Zhang, R. Clérac, *Inorg. Chem.* **2009**, *48*, 1606–1612.

[8] Crystal data and details of the X-ray diffraction experiment are in the Supporting Information. Further details on the crystal structure investigations may be obtained from the Fachinformationszentrum Karlsruhe, 76344 Eggenstein-Leopoldshafen, Germany (fax: (+49) 7247-808-666; e-mail: crysdata@fiz-karlsruhe.de), on quoting the depository number CSD-422363.

[9] I. D. Brown, D. Altermatt, *Acta Crystallogr. Sect. B* **1985**, *41*, 244–247.

[10] a) J. S. Anderson, *Nature* **1937**, *140*, 850; b) H. T. Evans, Jr., *J. Am. Chem. Soc.* **1948**, *70*, 1291–1292; c) H. T. Evans, Jr., *Acta Crystallogr. Sect. B* **1974**, *30*, 2095–2100.

[11] a) W. Schmitt, E. Baissa, A. Mandel, C. E. Anson, A. K. Powell, *Angew. Chem.* **2001**, *113*, 3689–3693; *Angew. Chem. Int. Ed.* **2001**, *40*, 3577–3581; b) J. C. Goodwin, S. J. Teat, S. L. Heath, *Angew. Chem.* **2004**, *116*, 4129–4133; *Angew. Chem. Int. Ed.* **2004**, *43*, 4037–4041.

[12] Examples include: a) J. L. Atwood, P. C. Junk, *Polyhedron* **2000**, *19*, 85–91; b) K. R. Fewings, P. C. Junk, D. Georganopoulou, P. D. Prince, J. W. Steed, *Polyhedron* **2001**, *20*, 643–649; c) X. Hao, M. A. Siegler, S. Parkin, C. P. Brock, *Cryst. Growth Des.* **2005**, *5*, 2225–2232; d) D. Braga, M. Gandolfi, M. Lusi, M. Polito, K. Rubini, F. Grepioni, *Cryst. Growth Des.* **2007**, *7*, 919–924.

[13] I. A. M. Pohl, L. G. Westin, M. Kritikos, *Chem. Eur. J.* **2001**, *7*, 3438–3445.

[14] N. Lima, A. Canschi, D. Gatteschi, M. Kritikos, D. G. Westin, *Inorg. Chem.* **2006**, *45*, 2391–2393.

[15] a) B. Keita, P. Mialane, F. Sécheresse, P. de Oliveira, L. Nadjo, *Electrochem. Commun.* **2007**, *9*, 164–172; b) F. M. Toma, A. Sartorel, M. Iurlo, M. Carraro, P. Parisse, C. Maccato, S. Rapino, B. R. Gonzalez, H. Amenitsch, T. Da Ros, L. Casalis, A. Goldoni, M. Marcaccio, G. Scorrano, G. Scoles, F. Paolucci, M. Prato, M. Bonchio, *Nat. Chem.* **2010**, *2*, 826–831; c) M. W. Kanan, D. G. Nocera, *Science* **2008**, *321*, 1072–1075; d) Y. Surendranath, M. W. Kanan, D. G. Nocera, *J. Am. Chem. Soc.* **2010**, *132*, 16501–16509.

[16] K. Hikaru, *J. Phys. Condens. Matter* **1998**, *10*, 4707–4754.

[17] M. F. Collins, O. A. Petrenko, *Can. J. Phys.* **1997**, *75*, 605–655.

[18] a) S. S. Mal, U. Kortz, *Angew. Chem.* **2005**, *117*, 3843–3846; *Angew. Chem. Int. Ed.* **2005**, *44*, 3777–3780; b) S. S. Mal, B. S. Bassil, M. Ibrahim, S. Nellutla, J. van Tol, N. S. Dalal, J. A. Fernández, X. López, J. M. Poblet, R. Ngo Biboum, B. Keita, U. Kortz, *Inorg. Chem.* **2009**, *48*, 11636–11645; c) S. S. Mal, M. H. Dickman, U. Kortz, A. M. Todea, A. Merca, H. Bögge, T. Glaser, A. Müller, S. Nellutla, N. Kaur, J. van Tol, N. S. Dalal, B. Keita, L. Nadjo, *Chem. Eur. J.* **2008**, *14*, 1186–1195.

[19] M. Ibrahim, Y. Lan, B. S. Bassil, Y. Xiang, A. Suchopar, A. K. Powell, U. Kortz, *Angew. Chem.* **2011**, *123*, 4805–4808; *Angew. Chem. Int. Ed.* **2011**, *50*, 4708–4711.

[20] *Inorganic Syntheses*, *Vol. 27* (Ed.: A. P. Ginsberg), Wiley, New York, **1990**, p. 87.

 © 2011 Wiley-VCH Verlag GmbH & Co. KGaA, Weinheim

Angewandte Chemie
Eine Zeitschrift der Gesellschaft Deutscher Chemiker

Supporting Information

© Wiley-VCH 2011

69451 Weinheim, Germany

A Planar $\{Mn_{19}(OH)_{12}\}^{26+}$ Unit Incorporated in a 60-Tungsto-6-Silicate Polyanion**

Bassem S. Bassil, Masooma Ibrahim, Rami Al-Oweini, Marie Asano, Zhenxing Wang, Johan van Tol, Naresh S. Dalal, Kwang-Yong Choi, Rosa Ngo Biboum, Bineta Keita, Louis Nadjo, and Ulrich Kortz**

anie_201007617_sm_miscellaneous_information.pdf

Supporting Information

1. Experimental details

General methods and materials. The reagents were used as purchased without further purification. The crystal water content was determined by thermogravimetric analysis (TGA) on a TA Instruments Q 600 device. Infrared spectra were recorded on KBr disks using a Nicolet-Avatar 370 spectrometer. Elemental analyses for Na, Si, W and Mn were performed by KANTI Labs in Tirupathi, India.

Crystal data for $Na_{34}[Mn_{19}(OH)_{12}(SiW_{10}O_{37})_6]\cdot 115H_2O$ (Na-1): A brown rod of **Na-1** with dimensions 0.40 x 0.16 x 0.08 mm^3 was mounted on a Hampton cryo-loop for indexing and intensity data collection at 173 K on a Bruker D8 APEX II CCD using Mo-Kα radiation (λ = 0.71073 Å). Of the 270926 reflection collected ($2\theta_{max}$ = 43.97, 98.6% complete), 18913 were unique (R_{int} = 0.1052) and 13005 reflections were considered observed (I > 2σ(I)). Lorentz and polarization corrections were applied, and an absorption correction was performed using the SADABS program (G. M. Sheldrick, Siemens Analytical X-ray Instrument Division: Madison, WI, 1995). Direct methods were used to locate the tungsten atoms (SHELXS-97). Then the remaining atoms were found from successive Fourier maps (SHELXL-97). The final cycle of refinement, including the atomic coordinates and anisotropic thermal parameters (Na, Mn, Si, and W atoms) converged at R = 0.0643 (I > 2 σ (I)) and R_w = 0.2148 (all data). In the final difference map the deepest hole was -4.268 $eÅ^{-3}$ and the highest peak 3.262 $eÅ^{-3}$.

Magnetism

DC magnetic susceptibility measurements on a powder sample of **Na-1** were carried out on a Quantum Design MPMS SQUID magnetometer at 0.02 T and in a temperature range of 1.8 - 300 K. The data were corrected for the diamagnetism with Klemm constants but not for any temperature-independent paramagnetism (TIP) contributions.[1] Magnetization of the sample as a function of magnetic field was measured at 1.8 K. The high frequency EPR spectra were obtained at 240 GHz on the superheterodyne quasioptical EPR spectrometer, which is located at the National High Magnetic Field Laboratory in Tallahassee, Florida, USA.[2,3] The spectrometer has a 12.5 T superconducting magnet (Oxford Instruments) and is equipped with an Oxford continuous helium flow cryostat with a temperature range of 1.5 – 400 K and a precision of 0.1 K.

[1] S. G. Vulfson, *Molecular Magnetochemistry*, Gordon and Breach Science: Newark, NJ, **1998**, 241.

[2] B. Cage, A. K. Hassan, L. Pardi, J. Krzystek, L.-C. Brunel, N. S. Dalal, *J. Magn. Reson.* **1997**, *124*, 495-498.

[3] A. K. Hassan, L. A. Pardi, J. Krzystek, A. Sienkiewicz, P. Goy, M. Rohrer, L.-C. Brunel, *J. Magn. Reson.* **2000**, *142*, 300-312.

Electrochemistry

Electrochemistry materials, apparatus and procedures. For electrochemical experiments, the source, mounting and polishing of the glassy carbon (GC) electrodes (Le Carbone Lorraine, France) have been described previously.[1] The electrochemical set-up was an EG & G 273 A driven by a PC with the M270 software. Potentials are measured against a saturated calomel reference electrode (SCE). The counter electrode was a platinum gauze of large surface area. Pure water from a RiOs 8 unit followed by a Millipore-Q Academic purification set was used throughout. The solutions were deaerated thoroughly for at least 30 minutes with pure argon and kept under a positive pressure of this gas during the experiments. The composition of the aqueous medium was 1 M CH_3COOLi + CH_3COOH (pH 5).

Electrochemistry of 1

The electrochemical behaviour of **1** was studied in an aqueous pH 5 medium. For clarity, the processes observed in the negative and positive potential domains (vs. SCE) are described separately. In the negative domain the cyclic voltammogram (CV) of **1** shows two well-defined waves at respectively -0.850 V and -0.960 V attributed to the reduction of the W^{VI} centers (Figure S3A). The last W-wave (not shown) is irreversible and close to the electrolyte discharge limit. Figure S3B shows the CV of the first redox processes of tungsten centers as a function of the potential scan rate. The variation of the W-reduction peak current as a function of the square root of the potential scan rate is also shown in Figure S3B (inset). The good linearity of this curve indicates that the first W-wave of **1** is diffusion-controlled. Perfect reproducibility of CVs was observed even after prolonged potential cycling. In the absence of oxygen, controlled potential coulometry indicates that the reduced form associated with the first W-redox couple is already active for the hydrogen evolution reaction. The reduction continues even after the consumption of more than 243 electrons per molecule. However, the cyclic voltammetric characteristics of **1** are preserved, a proof of electrocatalytic turnover of the system. The main redox characteristic features of the Mn(II) centers between -0.400V and +1.320 V vs SCE are represented in Figure S4. In this figure, the oxidation pattern is comprised of two chemically reversible waves peaking respectively at ca. +0.500V and +0.740 V vs SCE and followed by large intensity wave. The first two are attributed to stepwise oxidation of Mn(II) centers into Mn(IV) state through Mn(III) state in agreement with previous literature results.[2a] Controlled potential coulometry performed at + 0.830 V vs. SCE indicates the consumption of 2.00 ± 0.05 electrons per Mn, thus confirming that all the manganese centers in **1** are electroactive and have a +2 oxidation state. The third wave is mainly attributed to water oxidation.[2a] The overall reaction of interest is:

$O_2 + 4 H^+ + 4e^- \rightleftharpoons 2 H_2O \quad E_{anodic} = 1.23 - 0.059\ (pH)$ V vs. NHE

The current density for the water oxidation process was measured as a function of overpotential. The corresponding Tafel analysis (Figure S4B) was established with a scan rate of 2 mV s^{-1}. A good linearity

was observed between an overpotential of 330 mV to 600 mV. Except for a slight difference in the pH of the respective solutions (pH 5 vs. pH 7), this observation coincides roughly with two results published recently: the first one uses nanotube / Ru-containing polyoxometalate electrocatalytic interfaces for water oxidation[2b] and the second one is devoted to an oxygen evolving catalyst containing phosphate and Co^{2+}.[2c] In contrast, the slope of the Tafel line in our example stands in between those which could be estimated from the figures in these two papers: our value (135±10 mV / decade), is rather close to the roughly 83 mV / decade for the Co-oxide catalyst[2c] but is much smaller than the 310 mV / decade observed with the polyoxometalate deposited on nanotubes.[2b] Two conclusions emerge from this comparison: i)small Tafel slope is associated with simple oxides deposited on electrodes; ii) the POM of the present work shows more favourable oxygen evolution kinetics than the Ru-containing one.

For easier comparison with literature, the potentials measured with a saturated calomel electrode are converted to the NHE. In practice, the potential required for the OER at several current densities was compared with analogous literature values: at a current density of 1 mA cm^{-2} (v = 50 mV s^{-1}), the necessary overpotential is 445 mV, a figure close to the 410 mV announced by Nocera et al.;[2c] the extrapolated 1.8 V potential value in this paper for 5 mA cm^{-2} is measured to be 1715 mV in the case of the present POM; finally, for a 10 mA cm^{-2} current density, our experiments give 1745 mV compared to the 1770 mV observed on a rotating disc electrode in 0.5 M KOH medium.[2d] In short, taking into account the diversity of experimental conditions, the polyanion **1** displays very competitive kinetic parameters as concerns the OER. In addition, this catalyst is very durable and could be cycled hundreds of time without deactivation. A very thin film is deposited on the electrode surface either during potential cycling or electrolysis in agreement with previous literature results.[2a]

References

[1] B. Keita, L. Nadjo, *J. Electroanal. Chem*. **1988**, *243*, 87.

[2] a) B. Keita, P. Mialane, F. Sécheresse, P. de Oliveira, L. Nadjo, *Electrochem. Commun.*, **2007**, 9, 164-172; b) F.M. Toma, A. Sartorel, M. Iurlo, M. Carraro, P. Parisse, C. Maccato, S. Rapino, B. R. Gonzalez, H. Amenitsch, T. Da Ros, L. Casalis, A. Goldoni, M. Marcaccio,G. Scorrano, G. Scoles, F. Paolucci, M. Prato, M. Bonchio, *Nature Chemistry*, **2010**, 2, 826-831;c) M. W. Kanan, D.G. Nocera, *Science*, **2008**, 321, 1072-1075; d) Y. Gorlin, T.F. Jaramillo, *J. Am. Chem. Soc.*, **2010**, 132, 13612-13614.

Table S1. Bond valence sum values for oxygen and manganese atoms in {Mn_{19}} core in $Na_{34}[Mn_{19}(OH)_{12}(SiW_{10}O_{37})_6]\cdot 115H_2O$ (**Na-1**).

μ_3-O (3Mn–O)	**BVS value**	**Mn (6-coord.)**	**BVS value**
O10M	1.17	Mn1	2.21
O27M	1.17	Mn2	2.17
O58M	1.15	Mn3	2.24
O70M	1.12	Mn4	2.26
O80M	1.13	Mn5	2.14
O79M	1.11	Mn6	2.10
μ_4-O (3Mn–O–W)	**BVS value**	Mn9	1.88
O7A	2.04	**Mn (7-coord.)**	**BVS value**
O10A	2.06	Mn7	1.96
O17A	2.07	Mn8	1.96
O28A	2.04	Mn10	1.87
O29A	1.99		
μ_3-O (2Mn–O–W)	**BVS value**		
O8A	2.16		
O18A	1.91		
O19A	2.02		
O30A	2.02		

Table S2. Crystal data for $Na_{34}[Mn_{19}(OH)_{12}(SiW_{10}O_{37})_6]\cdot 115H_2O$ (**Na-1**).

Compound	**Na-1**
Empirical formula	$Na_{34}[Mn_{19}(OH)_{12}(SiW_{10}O_{37})_6]\cdot 115H_2O$
Formula weight, g/mol	18853.00
Crystal system	Triclinic
Space group	*P-1*
a, Å	16.1359(6)
b, Å	23.5734(10)
c, Å	24.7172(17)
α,°	112.039(3)
β,°	100.018(3)
γ.°	107.583(2)
Volume, $Å^3$	7856.3(7)
Z	1
D_{calc}, g/cm^3	3.985
Absorption coefficient	22.793
F(000)	8407
Crystal size, mm	0.40 x 0.16 x 0.08
Theta range for data collection, °	2.59- 23.27
Reflections collected	270926
Independent reflections	18913
R(int)	0.1052
Observed ($I > 2\sigma(I)$)	13005
T_{min} / T_{max}	0.222
Goodness-of-fit on F2	1.004
$R_1[I > 2\sigma(I)]$[a]	0.0643
wR_2 (all data)[b]	0.2148

[a] $R = \Sigma||F_o| - |F_c||/\Sigma|F_o|$. [b] $R_w = [\Sigma w(F_o^2 - F_c^2)^2/\Sigma w(F_o^2)^2]^{1/2}$.

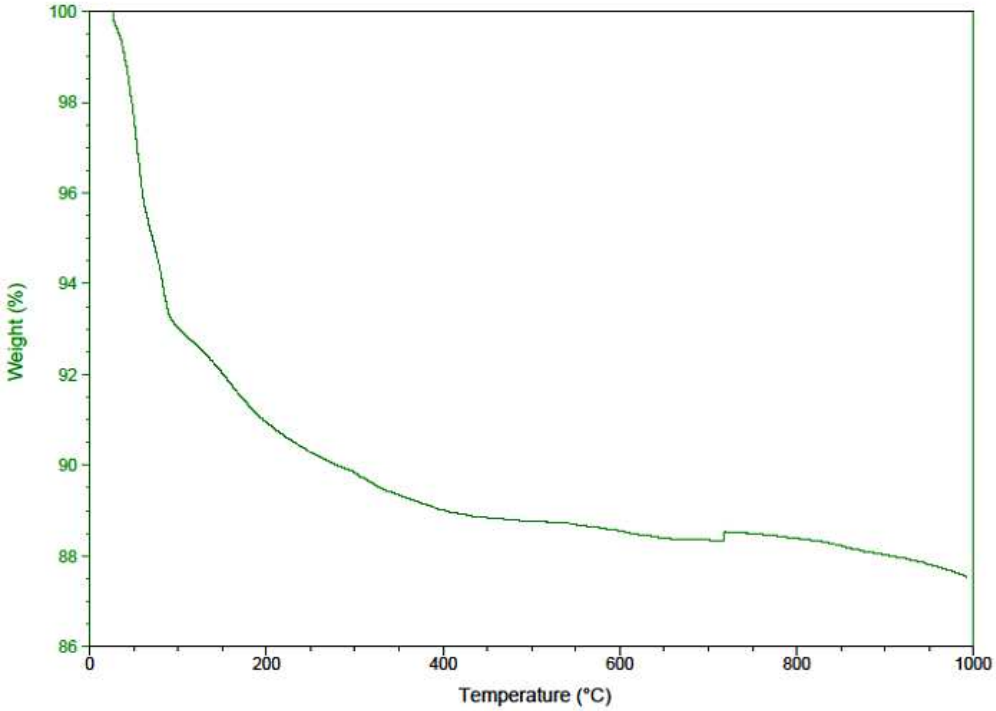

Figure S1. Thermogram of **Na-1** from room temperature to 1000 °C.

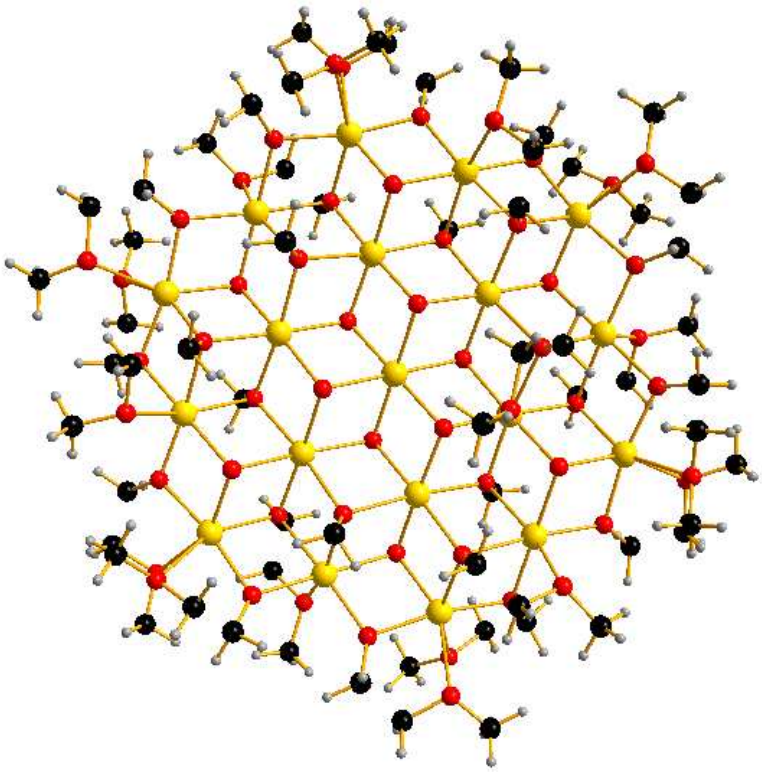

Figure S2. Ball-and-stick representation of Westin's $[Mn_{19}O_{12}(moe)_{14}(moeH)_{10}]$ ({Mn_{19}org}). See main text for details. Color code of balls: Mn yellow, O red, C black, H grey.

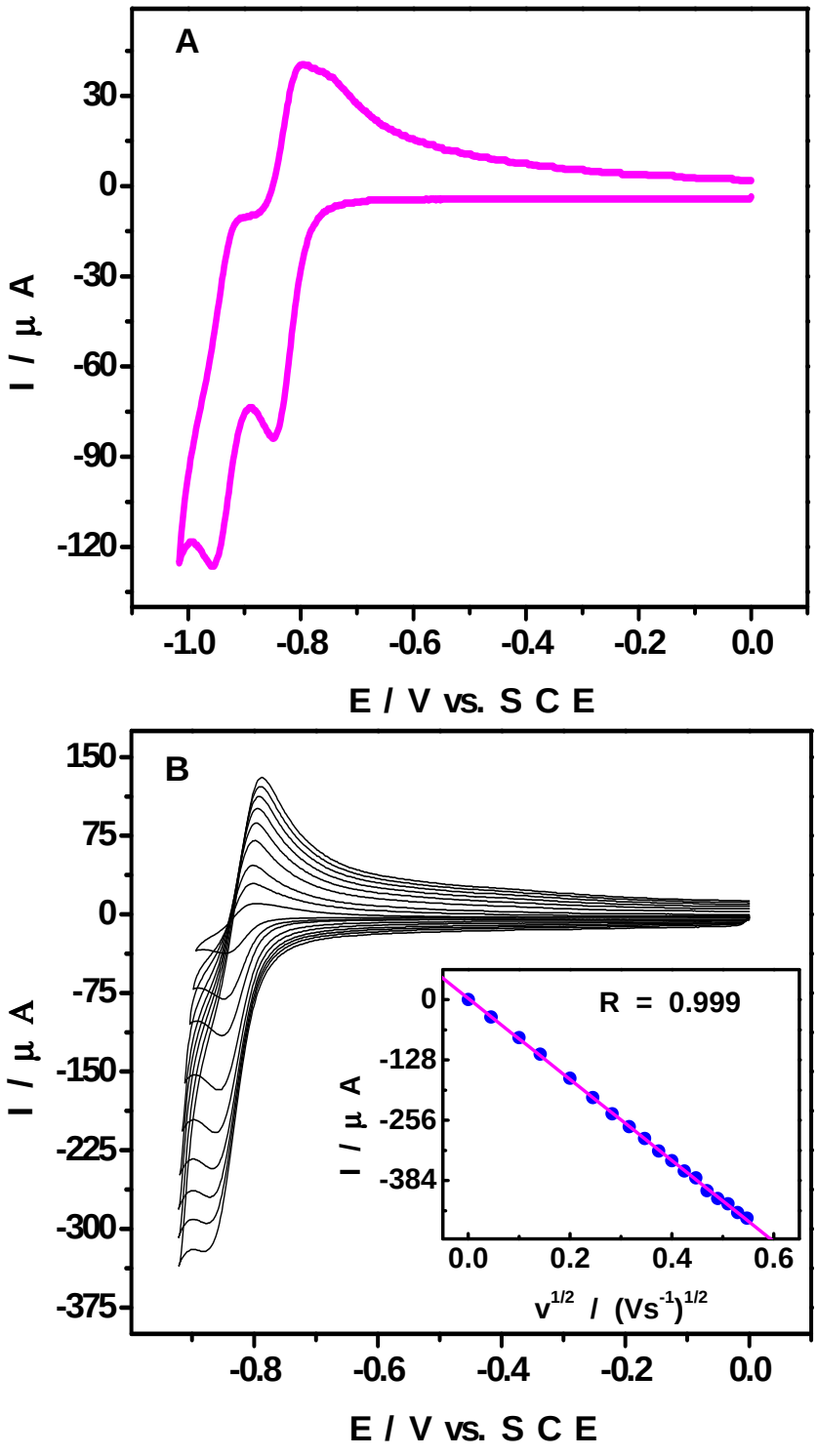

Figure S3. Cyclic voltammograms (CVs) and peak current intensity variations of 4 x 10^{-5} M **1** in a pH 5 medium (1M CH_3COOLi/CH_3COOH). The reference electrode was a saturated calomel electrode (SCE). (A) CV of the first two W^{VI}-waves. The scan rate was 10 mVs^{-1}. (B) CV of the first W^{VI}-wave as a function of scan rate (from inner to outer curve: 2, 10, 20, 40, 60, 80, 100, 120 and 140 mV s^{-1}, respectively); (inset) variation of the cathodic peak current intensity of the first W^{VI}-wave of **1** as a function the square root of the scan rate.

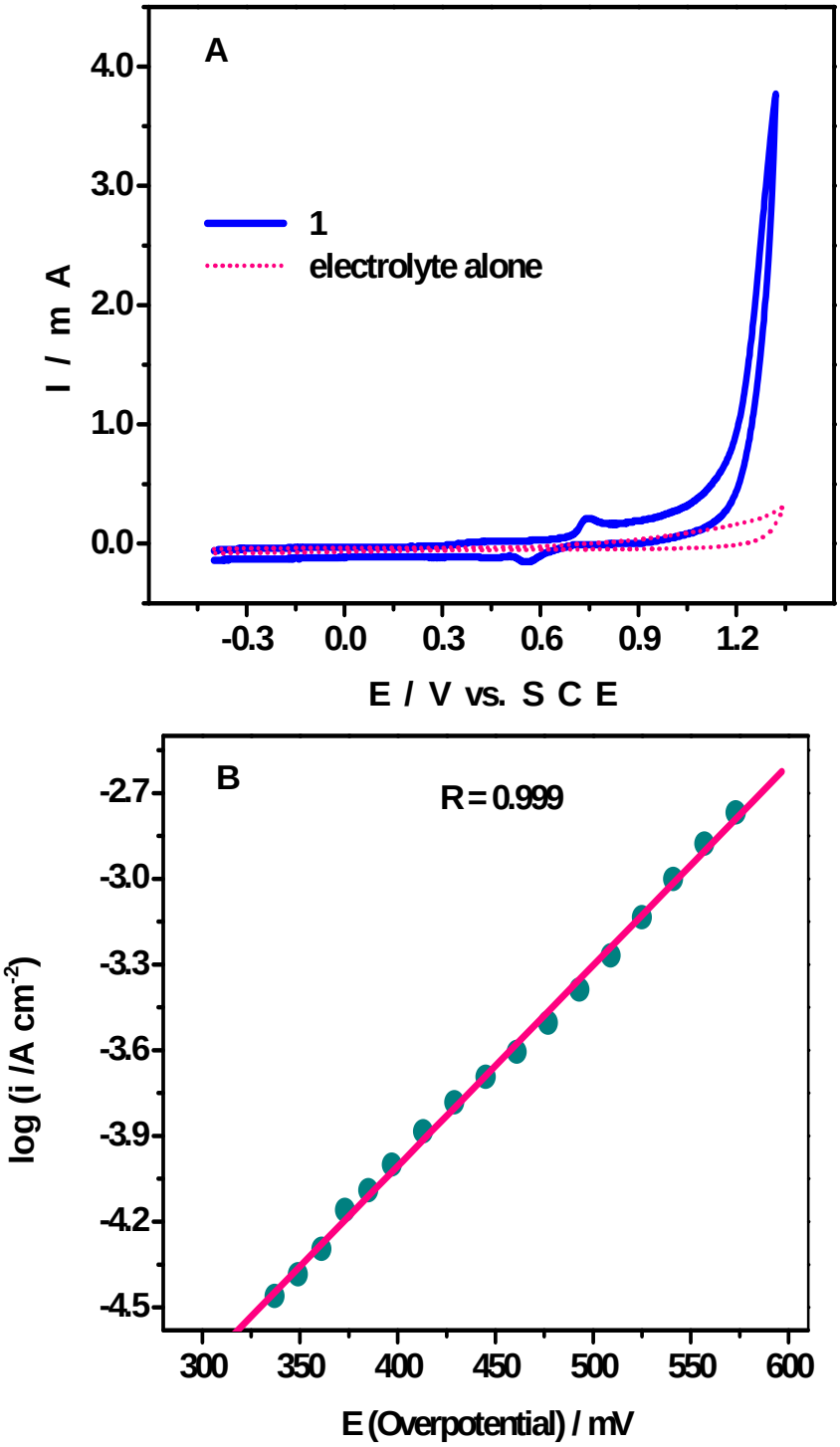

Figure S4. Redox activity of the Mn^{2+} centers of 4 x 10^{-5} M **1** in a pH 5 medium (1M CH_3COOLi/CH_3COOH).The reference electrode was a saturated calomel electrode (SCE). (A) dotted pink line: background current; full blue line: CV recorded in the presence of **1**. The scan rate was 10 mVs^{-1}. (B) Tafel polarization curve for the oxygen evolution reaction (OER). The scan rate was 2 mVs^{-1}. The current density i in the Tafel equation ($\eta = a + b \log i$, where η is the applied overpotential, b the Tafel slope) was expressed in ampere per unit of electrode real surface area.

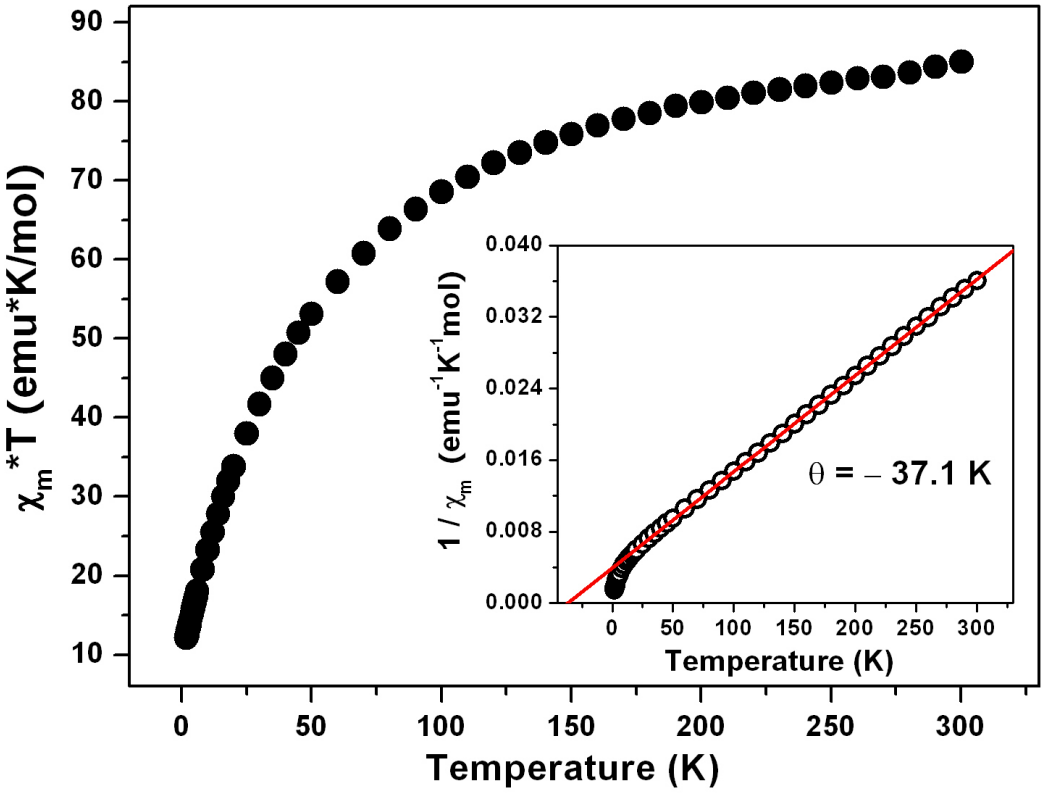

Figure S5. Plot of $\chi_m T$ for a polycrystalline sample of **Na-1** measured in an applied magnetic field of 0.02 T. Inset: $1/\chi_m$ as a function of temperature with a fit of the Curie-Weiss law based on the data of 50-300 K (red solid line).

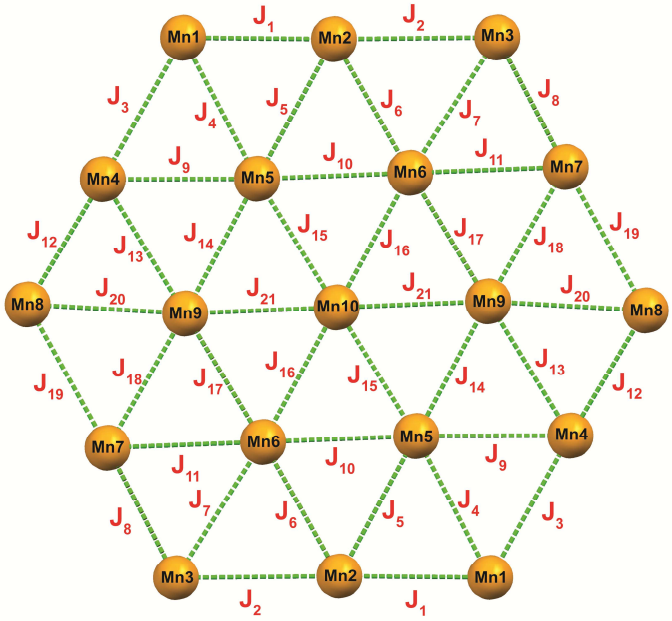

Figure S6. Spin topology of the Mn_{19} core in polyanion **1**.

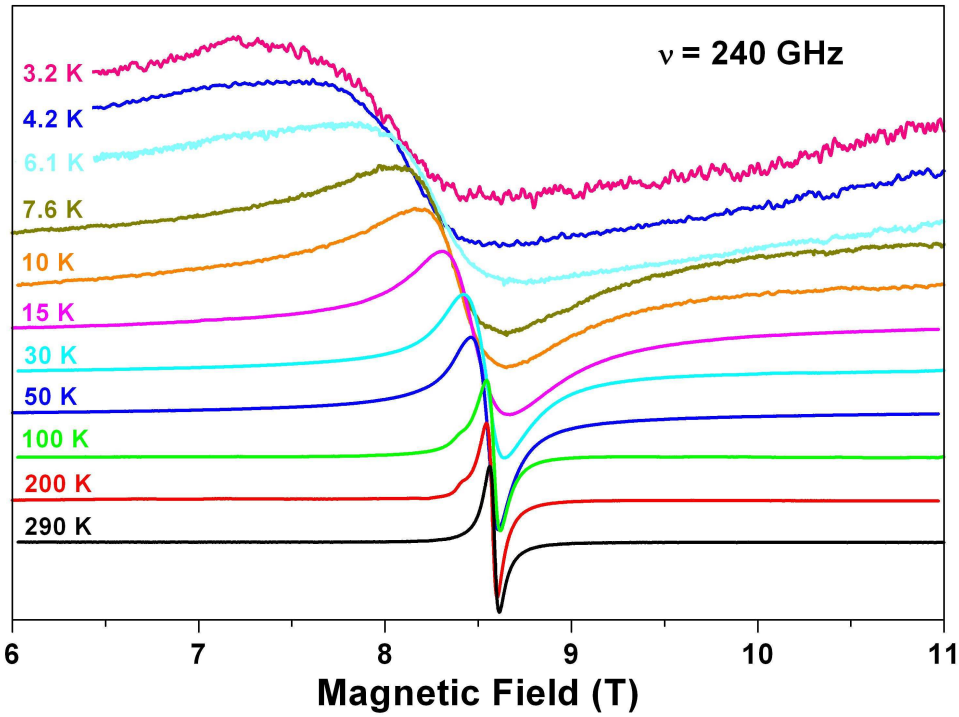

Figure S7. EPR spectra of a powder sample of **Na-1** at 240 GHz and various temperatures.

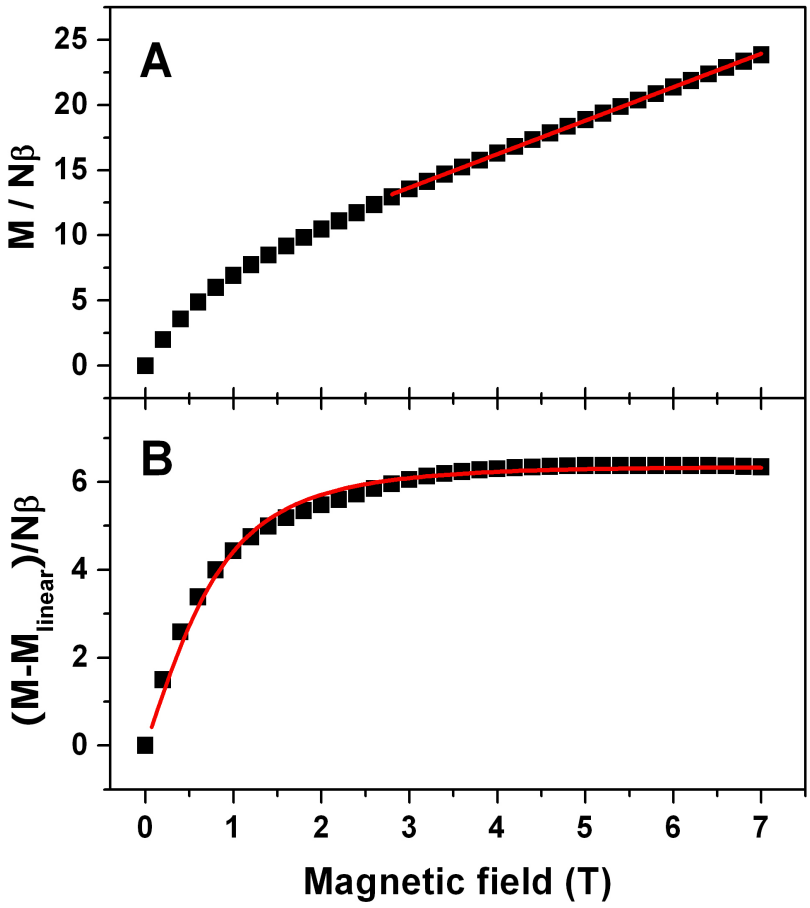

Figure S8. (A) Field dependence of magnetization of **Na-1** at 1.8 K; (B) Nonlinear part of *M(H)*. The continuous line is the fit to a modified Brillouin function $B_{5/2}$:[1]

$$M - B\frac{\partial M}{\partial B}|_{7T} = M_S B_{5/2}\left(\frac{M_S(\frac{\xi}{a})^2 H}{k_B T}\right)$$

where M_S is the saturation moment of the nonlinear part, ξ is the correlation length of the Mn^{II} spins, and a is the lattice parameter. The solid line is the resulting fit. The saturation moment of M_S = 6.2 μ_B is close to 5 μ_B expected for a saturation of one Mn^{II} ion. Further, we find that $\xi \approx 0.8a$. This suggests that an almost free spin is very weakly coupled to the remaining 18 spins with a correlation length of a lattice constant.

[1] S. G. Vulfson, *Molecular Magnetochemistry*, Gordon and Breach Science: Newark, NJ, **1998**, 241.

.

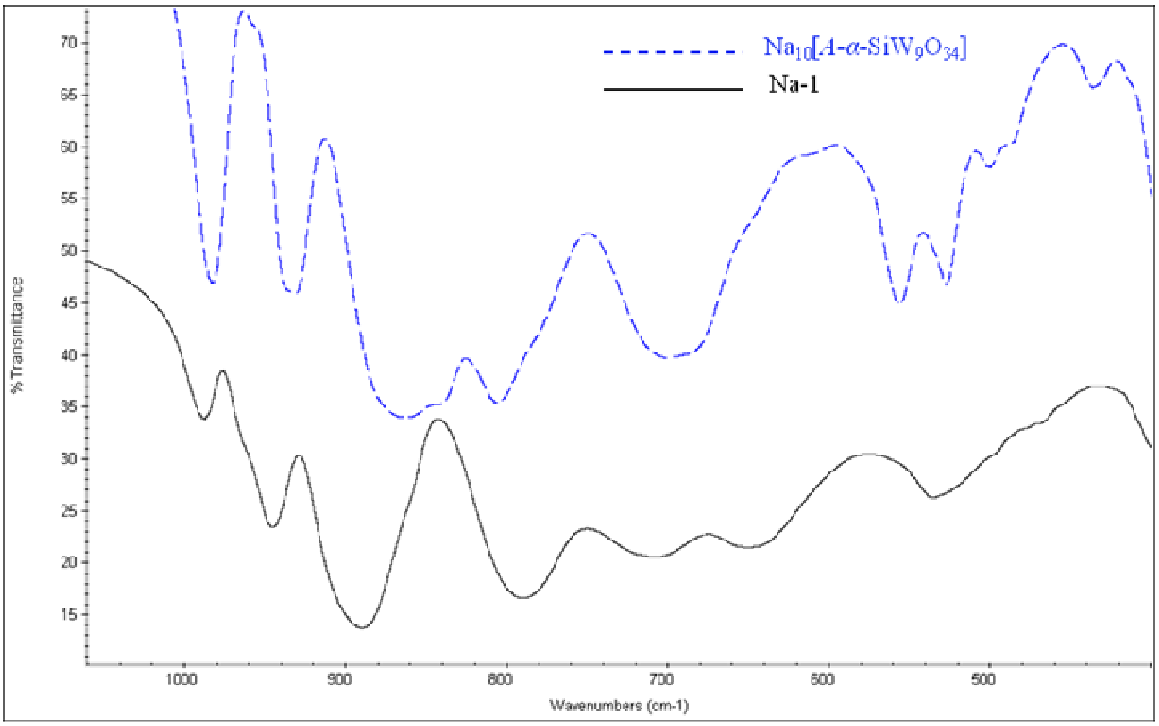

Figure S9. FT-IR spectra of $Na_{10}[A\text{-}\alpha\text{-}SiW_9O_{34}]$ precursor and **Na-1**.